HHS Public Access

Author manuscript

Angew Chem Int Ed Engl. Author manuscript; available in PMC 2023 August 26.

Published in final edited form as:

Angew Chem Int Ed Engl. 2023 May 02; 62(19): e202300289. doi:10.1002/anie.202300289.

Branched Multimeric Peptides as Affinity Reagents for the Detection of α-Klotho Protein

Xiyun Ye[+],
Department of Chemistry, Massachusetts Institute of Technology, 77 Massachusetts Avenue, 02139 Cambridge, MA (USA)

Dr. Peiyuan Zhang[+],
Department of Chemistry, Massachusetts Institute of Technology, 77 Massachusetts Avenue, 02139 Cambridge, MA (USA)

John C. K. Wang,
Calico Life Sciences, 1170 Veterans Boulevard, 94080 South San Francisco, CA (USA)

Dr. Corey L. Smith,
AbbVie Bioresearch Center, 100 Research Drive, 01605 Worcester, MA (USA)

Silvino Sousa,
AbbVie Bioresearch Center, 100 Research Drive, 01605 Worcester, MA (USA)

Dr. Andrei Loas,
Department of Chemistry, Massachusetts Institute of Technology, 77 Massachusetts Avenue, 02139 Cambridge, MA (USA)

Dr. Dan L. Eaton,
Calico Life Sciences, 1170 Veterans Boulevard, 94080 South San Francisco, CA (USA)

Dr. Magdalena Preciado López,
Calico Life Sciences, 1170 Veterans Boulevard, 94080 South San Francisco, CA (USA)

Prof. Dr. Bradley L. Pentelute
Department of Chemistry, Massachusetts Institute of Technology, 77 Massachusetts Avenue, 02139 Cambridge, MA (USA)

The Koch Institute for Integrative Cancer Research, Massachusetts Institute of Technology, 500 Main Street, Cambridge, 02142 MA (USA)

Center for Environmental Health Sciences, Massachusetts Institute of Technology, 77 Massachusetts Avenue, 02139 Cambridge, MA (USA)

blp@mit.edu, magdalena@calicolabs.com.
[+]These authors contributed equally to this work.

Conflict of Interest

B. L. P. is a co-founder and/or member of the scientific advisory board of several companies focusing on the development of protein and peptide therapeutics. A provisional patent disclosure was filed regarding the methodology and compounds described in this study.

Broad Institute of MIT and Harvard, 415 Main Street, 02142 Cambridge, MA (USA)

Abstract

α-Klotho, an aging-related protein found in the kidney, parathyroid gland, and choroid plexus, acts as an essential co-receptor with the fibroblast growth factor 23 receptor complex to regulate serum phosphate and vitamin D levels. Decreased levels of α-Klotho are a hallmark of age-associated diseases. Detecting or labeling α-Klotho in biological milieu has long been a challenge, however, hampering the understanding of its role. Here, we developed branched peptides by single-shot parallel automated fast-flow synthesis that recognize α-Klotho with improved affinity relative to their monomeric versions. These peptides were further shown to selectively label Klotho for live imaging in kidney cells. Our results demonstrate that automated flow technology enables rapid synthesis of complex peptide architectures, showing promise for future detection of α-Klotho in physiological settings.

Keywords

Flow Synthesis; Imaging Agents; Molecular Recognition; Protein–Protein Interaction; α-Klotho Protein

Introduction

The aging-related protein α-Klotho (hereinafter called Klotho) is a transmembrane protein, functioning as a co-receptor of fibroblast growth factor 23 (FGF23) with fibroblast growth factor receptors 1, 2, and 4 (FGFR).[1–4] The FGFR/Klotho/FGF23 complex regulates phosphate and calcium homeostasis in the kidney. Klotho has an extracellular domain composed of two tandem domains.[2] Cleavage of the extracellular domains produces a soluble form of Klotho released into circulation and found in the blood, urine, and cerebrospinal fluid.[4] Decreased membrane-bound or soluble Klotho protein levels are correlated with aging-related dysfunction, including diabetes, chronic kidney disease, cancers, and cardiovascular diseases.[4] The design of reagents with high affinity and selectivity for the detection of Klotho can help understand Klotho distribution in the body to facilitate early detection of aging-associating diseases and guide the development of anti-aging therapies.

Protein-protein interactions (PPIs) usually involve multivalent, cooperative interactions between two proteins to form tightly bound complexes.[5] Peptides can mimic the native binding epitope at PPI regions, thus capturing features of the extended molecular interaction.[6–8] Peptide-based affinity reagents are endowed with low molecular weight (<10 kDa), suitability for large-scale manufacture by solid-phase peptide synthesis, and enhanced stability in complex biological media. With these advantages, peptide reagents can be improved to penetrate cell membranes and potentially have a longer half-life and superior circulation profiles in vivo.[9–11]

The binding interface between Klotho and FGF23 provides opportunities for designing peptide-based agents targeting Klotho. The FGF23 N-terminus interacts primarily with

FGFR, while its C-terminus engages Klotho (Figure 1A).[2,12,13] The DiMarchi group identified peptides that mimic the C-terminus of FGF23 based on the minimal binding domain determined from the Klotho crystal structure[14] (Figure 1B). These peptides were able to antagonize the activity of FGF23 in cells. We selected a top-performing peptide (**Pep-10**, sequence: PMASDPLGVVRPRARM) and measured the binding affinity between **Pep-10-Biotin** (Figure S1) and recombinant mouse Klotho (mKlotho) using bio-layer interferometry (BLI). **Pep-10-Biotin** was immobilized onto the streptavidin tips. Serial dilutions of mKlotho were incubated with the tips to measure association and dissociation events, giving an apparent dissociation constant (K_D) of 2.3±0.5 μM (Figure S2A). The binding affinity of **Pep-10** is insufficient to detect Klotho in serum in the nanomolar range. However, **Pep-10** can serve as a promising starting point for developing peptide-based affinity reagents.

Results and Discussion

The preparation of multimeric, branched peptide reagents has been used to increase avidity while maintaining selectivity, effecting stronger binding affinity relative to the correspondent monomeric peptides.[15–17] However, the synthesis of branched peptides can be challenging due to the shared branching amino acid. Employing fast-flow synthesis with our in-house high-temperature automated synthesizer, we synthesized Klotho-binding branched peptides within half an hour, ranging from dimeric to tetrameric variants[18–20] (Figure 1C). During the flow synthesis, each step of fluorenylmethyloxycarbonyl (Fmoc) deprotection is monitored by in-line UV/Vis spectroscopy to ensure each synthesis cycle proceeds with high efficiency. Notably, the C-terminal residue of **Pep-10** is Met which introduces steric hindrance when elongating multiple peptide chains. To reduce the possibility of Met oxidation and potentially increase the synthesis yield, we used **KB1** (PMASDPLGVVRPRARA) instead of **Pep-10** (PMASDPLGVVRPRARM) as a monomer for the assembly of the branched peptides (Figure 2A). **KB1-Biotin** has a similar K_D to **Pep-10-Biotin** in the BLI assay, determined as 2.6±0.5 μM (Figure S2B). We accomplished the synthesis of each branch of the multimeric Klotho-binding peptides simultaneously through a parallel elongation process. After global deprotection and cleavage, the crude material was purified by high-performance flash chromatography (HPFC) and freeze-dried to obtain the pure branched peptides. For each synthesis batch, we obtained ≈4 μmol of pure material (16 mg of dimer **KB2**, 24 mg of trimer **KB3**, and 32 mg of tetramer **KB4**) in ≈20% yield starting from 20 μmol of Rink amide resin (Figure 1C).

To investigate whether branched multimeric peptides display improved binding affinity to Klotho, we applied analysis by high-performance size exclusion chromatography-mass spectrometry (HPSEC-MS), direct binding measurements by BLI, competitive binding assays by BLI, and fluorescence polarization (FP) assays. These biophysical assays demonstrated up to ~100-fold enhanced binding affinity towards Klotho by the branched multimeric peptides compared to monomer **KB1**.

HPSEC-MS analysis directly assesses the formation of the peptide-protein complex. Unlabeled peptides were individually mixed with Klotho and partitioned by HPSEC to separate protein-bound and unbound fractions. The eluted fraction corresponding to Klotho

was subsequently analyzed by mass spectrometry (MS) to confirm the recovery of bound branched peptides. **KB2** (recovery yield 4%, defined as the amount of peptide detected in the eluted Klotho fraction divided by the total amount of peptide used), **KB3** (recovery yield 3%), and **KB4** (recovery yield 2%) were retained in the Klotho fraction in three replicates (Figures 2 and S3). Notably, the parent **KB1** monomeric peptide was not observed in the Klotho fraction, indicating a potentially weaker interaction leading to dissociation of the complex on the SEC column. HPSEC-MS qualitatively showed enhanced binding to Klotho by the branched peptides relative to monomeric **KB1**.

Direct binding measurements by BLI were completed using **KB2-Biotin**, **KB3-Biotin**, and **KB4-Biotin**, in a similar manner to **KB1-Biotin**. These biotinylated probes were immobilized and immersed into solutions containing various concentrations of mKlotho at 1000, 500, 250, 125, 62.5, 31.3, 15.6, and 7.8 nM. The kinetic parameters, k_{on} (association rate constant) and k_{off} (dissociation rate constant), were then determined based on curve fitting, and the K_D value was calculated as k_{off}/k_{on}. Compared to the monomer **KB1** (K_D=2.6±0.5 μM), the branched peptides **KB2**, **KB3**, and **KB4** gave K_D values of 83±42 nM, 35±15 nM, and 88±56 nM, which resulted in 27.7, 65.7 and 26.1-fold improvements in affinity, respectively (Figures 2D and S2).

Competitive binding assays against the parent **KB1** binder allowed us to determine competition K_D values by BLI and confirmed Klotho site-specific binding by the branched multimeric variants. **KB1-Biotin** was immobilized onto the streptavidin biosensor tips. Increasing concentrations of unlabeled **KB1** through **KB4** were mixed with a constant concentration of mKlotho (100 nM) to measure binding and dissociation events. **KB1-Biotin**-immobilized tips were immersed into each of these solutions to estimate the fraction of unbound mKlotho and interpolate the competition K_D values. **KB1** competed off binding of mKlotho by **KB1-Biotin** and gave a competition K_D of 6.5±1.2 μM (Figure S4A). **KB2** (K_D=53±23 nM), **KB3** (K_D=75±29 nM), and **KB4** (K_D=139±43 nM) displayed progressively lower affinity (higher competition K_D values) with the increasing number of branches (Figures 2E and S4). Within the three branched peptides, the most significant improvement in binding affinity was observed with the dimer **KB2** in the competitive binding assays.

To assess the binding selectivity of **KB2**, we synthesized a control dimeric branched peptide based on a scrambled **KB2** sequence named **KB2-Scramble**. **KB2-Scramble** returned a high competition K_D (>10 μM) in the competitive binding assay (Figure 2E), indicating weak binding to mKlotho with at least 200-fold higher competition K_D. Therefore, **KB2-Scramble** was used as a negative control of **KB2** in downstream assays. Two additional proteins, MDM2 and 12CA5 were also used to evaluate the binding selectivity of **KB2**. Biotinylated probe **KB2-Biotin** displayed no association to these two proteins in the direct binding measurements by BLI (Figure S5). These results indicated the branched peptides showed non-promiscuous and site-specific binding interactions with Klotho.

We labeled **KB2** with the fluorophore 5-carboxytetramethylrhodamine (TAMRA) and determined its apparent dissociation constant K_D to be 154±24 nM, estimated by an FP assay (Figure S6). This orthogonal assay suggested fluorophore-labeled **KB2** retains

nanomolar binding affinity to Klotho. The binding affinities of **KB2-TAMRA** and **KB2-Scramble-TAMRA** were also evaluated in the competitive binding assays by BLI to provide a comparison to the unlabeled molecules (Figure S4D). The competition K_D of **KB2-TAMRA** was determined as 57±26 nM, which is similar to **KB2** (K_D=53±23 nM). As in the case of **KB2-Scramble** alone, **KB2-Scramble-TAMRA** displayed minimal binding to Klotho (K_D>10 μM). In summary, these findings ensured binding between **KB2** and Klotho is not affected upon modification with TAMRA.

To transition from the mKlotho used in the above binding assays to human Klotho (hKlotho), we measured the direct binding of **KB1-Biotin** to hKlotho by BLI. The experimentally determined K_D was 3.0±0.6 μM, similar to the value determined for **KB1-Biotin** binding to mKlotho (K_D=2.6±0.5 μM) (Figure S7A). Furthermore, **KB2** bound hKlotho with K_D=85±22 nM in the competitive binding assay by BLI (Figure S7B). This value is comparable to the competition K_D determined against mKlotho (K_D=53±23 nM) in the same assay (Figure 2E). Similarly, **KB2-TAMRA** displayed K_D=90±31 nM to hKlotho while **KB2-Scramble-TAMRA** returned a K_D>10 μM, indicating the attachment of TAMRA has no significant effect on **KB2**'s binding to hKlotho (Figure S7C and S7D).

These biophysical assays suggested that the lead dimer peptide **KB2** has an enhanced binding affinity towards Klotho compared to monomeric **KB1**. In the competition assays, the K_D of **KB1** is 6.5 μM which is 123-fold higher than the K_D of **KB2** (53 nM). Our flow synthesis technology delivered peptides with diverse branching architectures, including dimeric peptide **KB2**, which had the highest Klotho binding affinity and therefore was selected for downstream target engagement assays.

To study the engagement of Klotho in a complex cellular environment by **KB2**, we first investigated whether **KB2** can capture supplemented recombinant mKlotho from cell lysates. We added recombinant mKlotho into the cell lysate of CaSki cells, a human cervical cancer cell line that was reported to display minimal Klotho expression[21] (Figure S8), to a final concentration of 100 nM. Klotho was significantly enriched in the pulled-down fraction by **KB2-Biotin** starting at 200 nM, consistent with its binding affinity determined by BLI (Figure 3A). The **KB1-Biotin** and control probe **KB2-Scramble-Biotin** did not enrich mKlotho even at 1 μM (Figure 3A and S9). To confirm the protein enriched from lysate was Klotho, we ran a control pull-down with a commercially available Klotho antibody (KM2076). The pull-down fraction by **KB2-Biotin** and by Klotho antibody gave bands with the same molecular weight, confirming it was Klotho being enriched (Figure S9). In a self-competition assay, pull-down of Klotho by **KB2-Biotin** could be competed off by unlabeled **KB2** added to the cell lysate in a dose-dependent manner, but not by **KB2-Scramble** (Figure 3B). Together, the dose-dependent and the self-competition pull-down assays show direct mKlotho engagement by **KB2** in cell lysate. To investigate the selectivity of pull-down, the silver stain was performed on the pull-down eluents of **KB2-Biotin**. mKlotho was the only significantly enriched protein by **KB2-Biotin** at 200 nM but not by the negative control **KB2-Scramble-Biotin**, demonstrating selective pull-down achieved by **KB2-Biotin** (Figure S10). Next, we evaluated hKlotho engagement in human kidney 2 (HK-2), a proximal tubular cell line expressing detectable Klotho endogenous levels.[22] **KB2-Biotin** enriched

hKlotho from HK-2 cell lysate at 200 nM, but not **KB2-Scramble-Biotin** (Figure 3C). These studies demonstrate the direct binding of **KB2** to both recombinant mKlotho and endogenous hKlotho, supporting the notion that the branched multimeric peptide has the potential to engage its target in the biological milieu selectively.

Labeling specific proteins of interest in live cells remains challenging due to the general dearth of stable, selective affinity reagents that are not antibody-based. Since **KB2-TAMRA** selectively binds to Klotho with high affinity and selectivity, proved by the competition assay by BLI (Figure S4D), we used it as our lead Klotho affinity reagent for fluorescence microscopy imaging of HK-2 cells. A time course study was performed to optimize the imaging protocol, suggesting a robust intracellular fluorescence signal was obtained in fixed HK-2 cells upon incubation with 500 nM of **KB2-TAMRA** for only 5 min (Figure S11). The scrambled control, **KB2-Scramble-TAMRA**, did not display appreciable fluorescence emission in HK-2 cells, indicating minimal binding to Klotho and potential low internalization efficiency into cells (Figure S11). The cell membrane was demarcated in these assays with the membrane-specific dye Wheat Germ Agglutinin (WGA) Alexa Fluor™ 350 Conjugate. To validate that intracellular fluorescence comes from labeling Klotho by **KB2-TAMRA**, we performed several target engagement and competition studies using recombinant hKlotho and unlabeled **KB2** binder (Figure 4). Pre-incubation of **KB2-TAMRA** with recombinant hKlotho significantly decreased the intensity of the fluorescence signal, consistent with a reduced amount of free, unbound **KB2-TAMRA** available for cell labeling (Figure 4). We also validated that **KB2-TAMRA** and **KB2** engage the same binding site in cells by a competition experiment. Pretreatment of cells with **KB2** off-competed labeling of endogenous Klotho by **KB2-TAMRA**, resulting in significantly decreased intracellular fluorescence (Figure 4). This indicates that **KB2-TAMRA** and **KB2** bind the same site of Klotho in cells, consistent with the in vitro binding assay (Figure 2E and S7 C).

To further validate the selective binding, we knocked down endogenous Klotho levels in HK-2 cells with a pool of siRNAs (KL siRNA, Figure S12), followed by treatment with **KB2-TAMRA**. Mock transfection did not affect fluorescence in cells (Figure 5A) as expected. Notably, knocking down Klotho levels by KL siRNA reduced the fluorescence of **KB2-TAMRA**, supporting that fluorescent labeling by **KB2-TAMRA** is indeed Klotho-dependent (Figure 5).

We also investigated whether **KB2-TAMRA** can internalize and engage its target in a different cell line with lower Klotho expression levels. We incubated **KB2-TAMRA** with Klotho-deficient CaSki cells (Figure S8) using a similar protocol to HK-2 cells. Under these conditions, **KB2-TAMRA** exhibited a significantly lower fluorescence intensity in CaSki cells relative to Klotho-expressing HK-2 cells, potentially indicating reduced cell penetration and consistent with the expected lower Klotho levels (Figure S13A).

KB2-TAMRA selectively labels Klotho in endogenously Klotho-expressing cells. We then compared the fluorescence microscopy images of **KB2-TAMRA** with the Klotho antibody (KM2076, Figure S13B) under the same conditions. We found the fluorescence patterns to be similar, suggesting selective labeling of Klotho by **KB2-TAMRA**. To confirm this result, we used one additional Klotho antibody (MABN2398) and obtained fluorescence

patterns similar to KM2076 (Figure S13C). To monitor Klotho subcellular localization, we used DAPI to stain the cell nuclei (Figure S14). Pearson correlation coefficients (Pearson's *r*) were used to quantify the co-localization of nucleus dye DAPI versus **KB2-TAMRA** (Figure S14A) and Klotho antibody (Figure S14B). Low Pearson coefficients (*r* value of 0.29 for the overlap between DAPI and **KB2-TAMRA**, *r* value of 0.29 for the overlap between DAPI and Klotho antibody) indicated **KB2-TAMRA** and the Klotho antibody stain primarily the membrane, cytosol and intracellular organelles of HK-2 cells, but not significantly the nucleus. These results support membrane and cytoplasmic localization of Klotho consistent with the literature.[23] The Klotho antibody requires overnight incubation, followed by additional permeation steps and incubation with the secondary antibody, which makes it unsuitable for live cell labeling. On the contrary, our fluorescent peptide **KB2-TAMRA** could label Klotho in live HK-2 cells due to a short incubation time (5 min) and mild conditions (Figure S15). These imaging experiments support that **KB2-TAMRA** can potentially be used as an efficient and selective probe to label Klotho in both fixed and live cells.

Conclusion

We reported a flow synthesis strategy to deliver branched peptides as high-affinity reagents and selective probes to engage Klotho in a cellular context. Multiple biophysical and biochemical assays validated their binding affinities. These branched peptides were developed into fluorescent labeling agents with other potential uses. We show that the lead dimeric Klotho-binding peptide **KB2** selectively captures Klotho from cell lysates and can image endogenously expressed Klotho in fixed and live HK-2 cells when conjugated to a fluorophore.

The accessibility and availability of binding sites can affect affinity. The FGF23 protein contains two homologous tandem repeats, repeat 1 ($FGF23^{180–205}$) and repeat 2 ($FGF23^{212–239}$), which function as two distinct ligands for Klotho, implying the existence of two FGF23-association sites on Klotho.[12,14] Although further structural studies are needed, the branched Klotho-binding peptides may engage both FGF23 binding sites on Klotho, leading to binding enhancement.

In some cases, an increase in the degree of branching can increase affinity until the optimal binding is reached.[15,16] In the current case of Klotho/FGF23 interactions, the relative gain as the number of branches increases is limited by the availability of only two Klotho binding sites. This may be the reason that dimer **KB2** has a superior performance over **KB3** and **KB4**.

The accessibility of binding sites can be adjusted by varying the linkers between branches. In our study, we utilized an epsilon-lysine (ε-Lys) linker for this purpose. However, fine-tuning the geometry and length of linkers may significantly improve binding as further structural data on Klotho/FGF23 interactions become available. The current crystal structure (PDB: 5W21) only informs on such interactions up to the repeat 1 region of FGF23.

To further optimize the Klotho-targeting peptides, we envision a rational design strategy to affinity-mature the sequences, leading to improved biophysical properties. Optimization to further improve affinity, reduce molecular weight, and improve stability in vivo may pave the way for developing next-generation Klotho detection agents.

Supplementary Material

Refer to Web version on PubMed Central for supplementary material.

Acknowledgements

Calico Life Sciences (to B. L. P.) provided financial support for this work. We acknowledge support from the Swanson Biotechnology Center Microscopy Core Facility at the Koch Institute for Integrative Cancer Research at MIT through their epifluorescence microscope (NCI Cancer Center Support Grant P30-CA14051).

Data Availability Statement

The data that support the findings of this study are available either in the main text or in the supporting information of this article.

References

[1]. Lim K, Groen A, Molostvov G, Lu T, Lilley KS, Snead D, James S, Wilkinson IB, Ting S, Hsiao LL, Hiemstra TF, Zehnder D, J. Clin. Endocrinol. Metab. 2015, 100, E1308–E1318. [PubMed: 26280509]

[2]. Chen G, Liu Y, Goetz R, Fu L, Jayaraman S, Hu MC, Moe OW, Liang G, Li X, Mohammadi M, Nature 2018, 553, 461–466. [PubMed: 29342138]

[3]. Kuro-o M, Nat. Rev. Nephrol. 2019, 15, 27–44. [PubMed: 30455427]

[4]. Kim J-H, Hwang K-H, Park K-S, Kong ID, Cha S-K, J. Lifestyle Med. 2015, 5, 1–6. [PubMed: 26528423]

[5]. Valeur E, Guéret SM, Adihou H, Gopalakrishnan R, Lemurell M, Waldmann H, Grossmann TN, Plowright AT, Angew. Chem. Int. Ed. 2017, 56, 10294–10323; Angew. Chem. 2017, 129, 10428–10459.

[6]. Hillig RC, Sautier B, Schroeder J, Moosmayer D, Hilpmann A, Stegmann CM, Werbeck ND, Briem H, Boemer U, Weiske J, Badock V, Mastouri J, Petersen K, Siemeister G, Kahmann JD, Wegener D, Böhnke N, Eis K, Graham K, Wortmann L, Von Nussbaum F, Bader B, Proc. Natl. Acad. Sci. USA 2019, 116, 2551–2560. [PubMed: 30683722]

[7]. Bird GH, Mazzola E, Opoku-Nsiah K, Lammert MA, Godes M, Neuberg DS, Walensky LD, Nat. Chem. Biol. 2016, 12, 845–852. [PubMed: 27547919]

[8]. Grossmann TN, Yeh JTH, Bowman BR, Chu Q, Moellering RE, Verdine GL, Proc. Natl. Acad. Sci. USA 2012, 109, 17942–17947. [PubMed: 23071338]

[9]. Rezai T, Yu B, Millhauser GL, Jacobson MP, Lokey RS, J. Am. Chem. Soc. 2006, 128, 2510–2511. [PubMed: 16492015]

[10]. Walensky LD, Bird GH, J. Med. Chem. 2014, 57, 6275–6288. [PubMed: 24601557]

[11]. Muttenthaler M, King GF, Adams DJ, Alewood PF, Nat. Rev. Drug Discovery 2021, 20, 309–325. [PubMed: 33536635]

[12]. Suzuki Y, Kuzina E, An SJ, Tome F, Mohanty J, Li W, Lee S, Liu Y, Lax I, Schlessinger J, Proc. Natl. Acad. Sci. USA 2020, 117, 31800–31807. [PubMed: 33257569]

[13]. Pan J, Parlee SD, Brunel FM, Li P, Lu W, Perez-Tilve D, Liu F, Finan B, Kharitonenkov A, Dimarchi RD, ACS Pharmacol. Transl. Sci. 2020, 3, 978–986. [PubMed: 33073195]

[14]. Agrawal A, Ni P, Agoro R, White KE, DiMarchi RD, Cell Rep. 2021, 34, 108665. [PubMed: 33503417]

[15]. Wan J, Alewood PF, Angew. Chem. Int. Ed. 2016, 55, 5124–5134; Angew. Chem. 2016, 128, 5208–5219.

[16]. Brunetti J, Falciani C, Bracci L, Pini A, Pept. Sci. 2018, 110, e24089.

[17]. Molakaseema V, Selvaraj A, Chen HT, Chen YW, Liu YC, Kao CL, J. Org. Chem. 2022, 87, 1–9. [PubMed: 34677067]

[18]. Hartrampf N, Saebi A, Poskus M, Gates ZP, Callahan AJ, Cowfer AE, Hanna S, Antilla S, Schissel CK, Quartararo AJ, Ye X, Mijalis AJ, Simon MD, Loas A, Liu S, Jessen C, Nielsen TE, Pentelute BL, Science 2020, 368, 980–987. [PubMed: 32467387]

[19]. Mijalis AJ, Thomas DA, Simon MD, Adamo A, Beaumont R, Jensen KF, Pentelute BL, Nat. Chem. Biol. 2017, 13, 464–466. [PubMed: 28244989]

[20]. Pomplun S, Jbara M, Schissel CK, Wilson Hawken S, Boija A, Li C, Klein I, Pentelute BL, ACS Cent. Sci. 2021, 7, 1408–1418. [PubMed: 34471684]

[21]. Lee J, Jeong DJ, Kim J, Lee S, Park JH, Chang B, Il Jung S, Yi L, Han Y, Yang Y, Kim KI, Lim JS, Yang I, Jeon S, Bae DH, Kim CJ, Lee MS, Mol. Cancer 2010, 9, 109. [PubMed: 20482749]

[22]. Guan X, Nie L, He T, Yang K, Xiao T, Wang S, Huang Y, Zhang J, Wang J, Sharma K, Liu Y, Zhao J, J. Pathol. 2014, 234, 560–572. [PubMed: 25130652]

[23]. Xu Y, Sun Z, Endocr. Rev. 2015, 36, 174–193. [PubMed: 25695404]

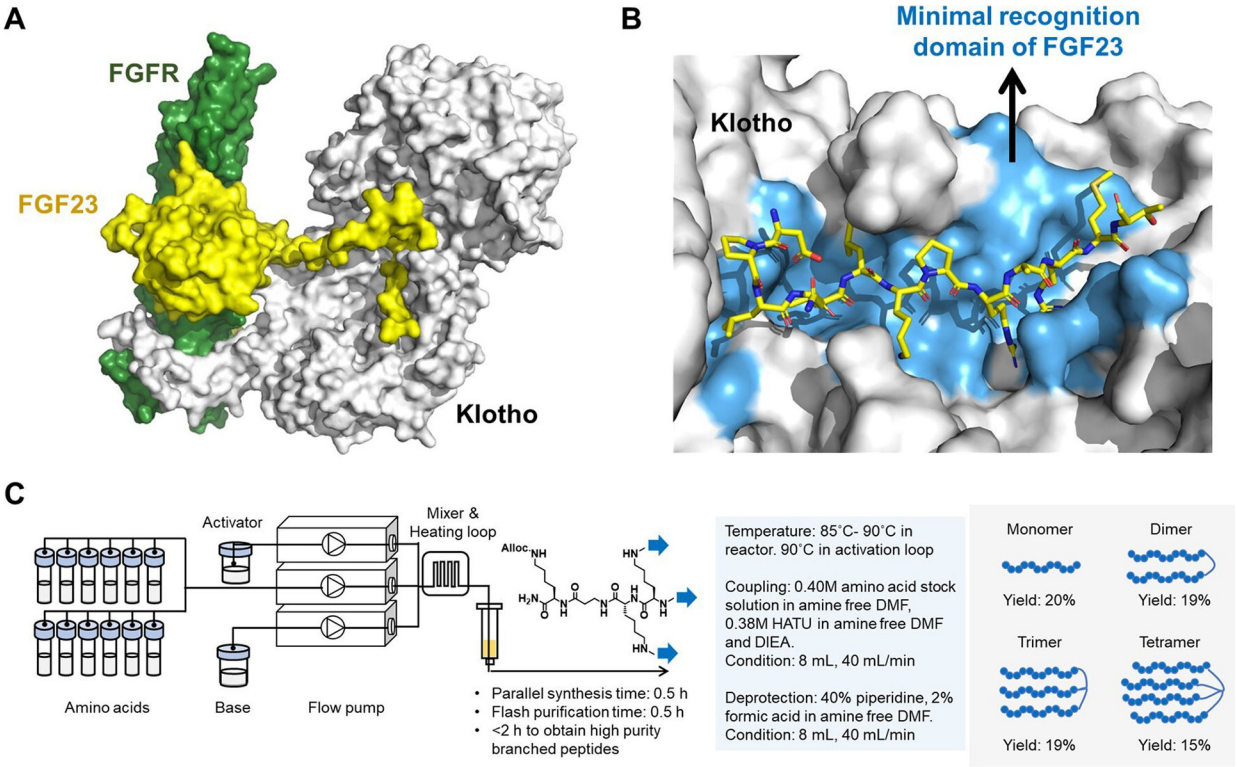

Figure 1.

Automated flow synthesis provided access to high-affinity peptide reagents to detect Klotho. (A) Structure of the protein-protein interaction between co-receptor protein Klotho, receptor protein FGFR, and signaling protein FGF23, modified from PDB: 5W21. Klotho is in white, FGFR protein is in green, and FGF23 is in yellow. (B) Visualization of the binding pocket of Klotho and the C-terminus of FGF23. $FGF23^{188–200}$ is shown as sticks, and the Klotho van der Waals protein surface is white. The contacting surface of Klotho is colored blue. (C) Schematic representation of an automated fast-flow protein synthesizer (AFPS) coupled to a flash chromatography system to synthesize branched peptides in parallel.

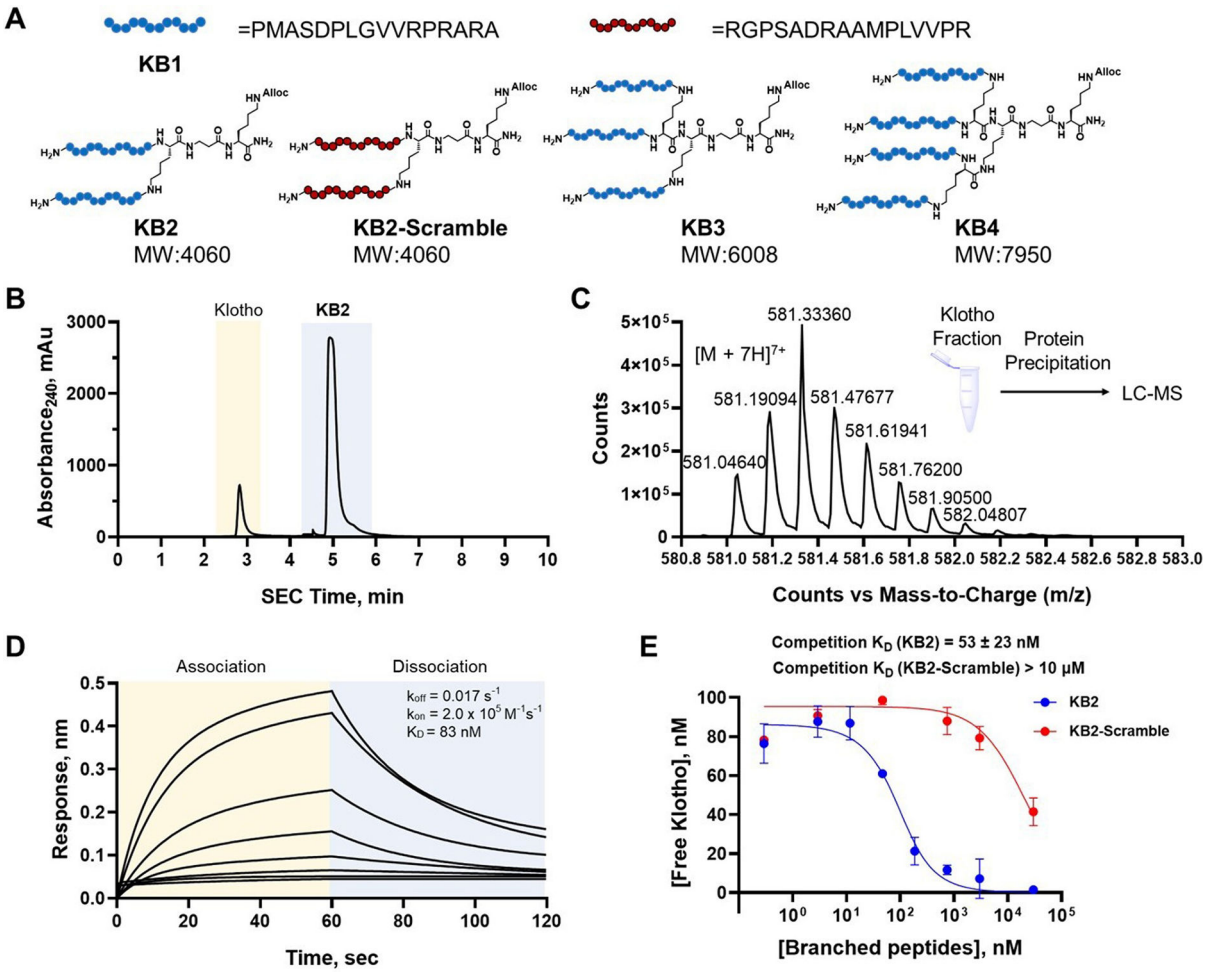

Figure 2.

Biophysical studies characterized the molecular interactions between branched multimeric peptide binders and Klotho. (A) The sequences and schematic representations of monomeric Klotho-binding peptide (**KB1**), dimeric Klotho-binding peptide (**KB2**), control scramble peptide (**KB2-Scramble**), trimeric Klotho-binding peptide (**KB3**), and tetrameric Klotho-binding peptide (**KB4**). (B) HPSEC-MS analysis of the Klotho–**KB2** complex. HPSEC achieved a baseline separation of the protein (1 μM, retention time 2.7 min) and peptide (10 μM, retention time 4.8 min) fractions. (C) The mass spectrum of **KB2** was detected in the protein fractions (peak with a retention time of 2.7 min in Figure 2B) after the precipitation of Klotho, indicating a strong peptide-protein interaction. (D) Analysis of the Klotho–**KB2-Biotin** interaction through a direct binding measurement by BLI. **KB2** was functionalized with Biotin-PEG4 using the preinstalled Alloc-handle to provide **KB2-Biotin**, which was further immobilized onto streptavidin tips. The solutions contained various concentrations of Klotho as 1000, 500, 250, 125, 62.5, 31.3, 15.6, and 7.8 nM. The direct binding was recorded by a BLI system to study the dissociation and association kinetics (n=2). The off-rate of **KB2-Biotin** was estimated to be 0.017 s^{-1}, and the on-rate was estimated to be $2.0 \cdot 10^5$ M^{-1} s^{-1}. (E) A competition assay by BLI was established to estimate the competitive dissociation constant (K_D) in a label-free format (n=2). Unlabeled **KB2** binds to Klotho with

K_D=53±23 nM. The control peptide **KB2-Scramble** does not significantly associate with Klotho (K_D>10 μM). Error bars indicate SD.

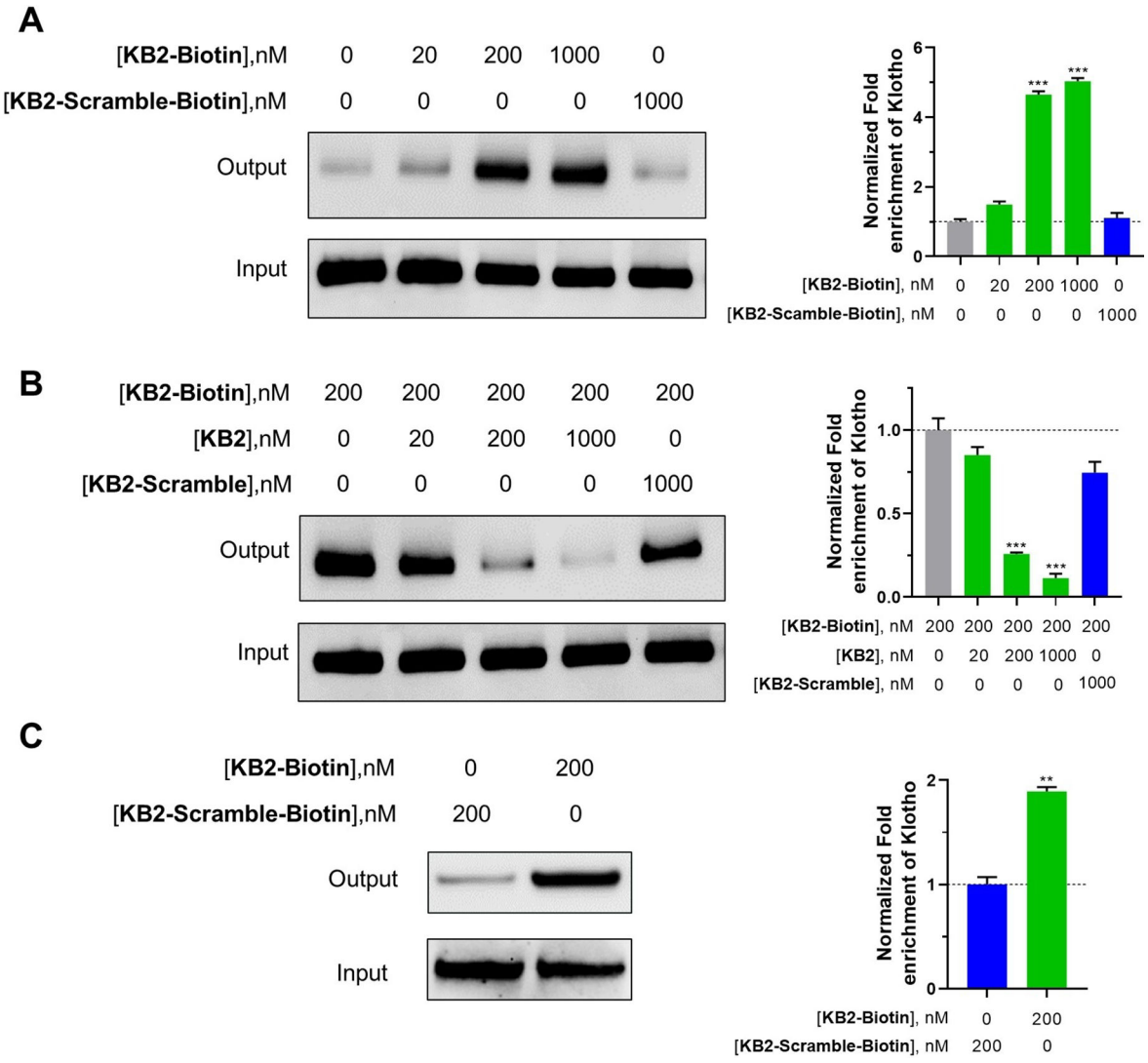

Figure 3.

Pull-down assays from human cell lysates showed direct Klotho engagement by **KB2**. (A) Pull-down probe **KB2-Biotin** enriched recombinant mKlotho from 100 μg of CaSki cell lysate in a dose-dependent manner. Control probe **KB2-Scramble-Biotin** displayed no enrichment of Klotho at 1 μM. The bar graph depicts the quantification of protein pull-down (n=2). (B) Pull-down of mKlotho by **KB2-Biotin** can be competed off by **KB2** in a dose-dependent manner, but not by **KB2-Scramble**. The bar graph depicts protein quantification in the competitive pull-down assay (n=2). (C) **KB2-Biotin** significantly enriched endogenous hKlotho from HK-2 cell lysate at 200 nM. The bar graph depicts the quantification of protein pull-down (n=2). ** P<0.01, *** P<0.001, as determined by ANOVA. Error bars indicate SD.

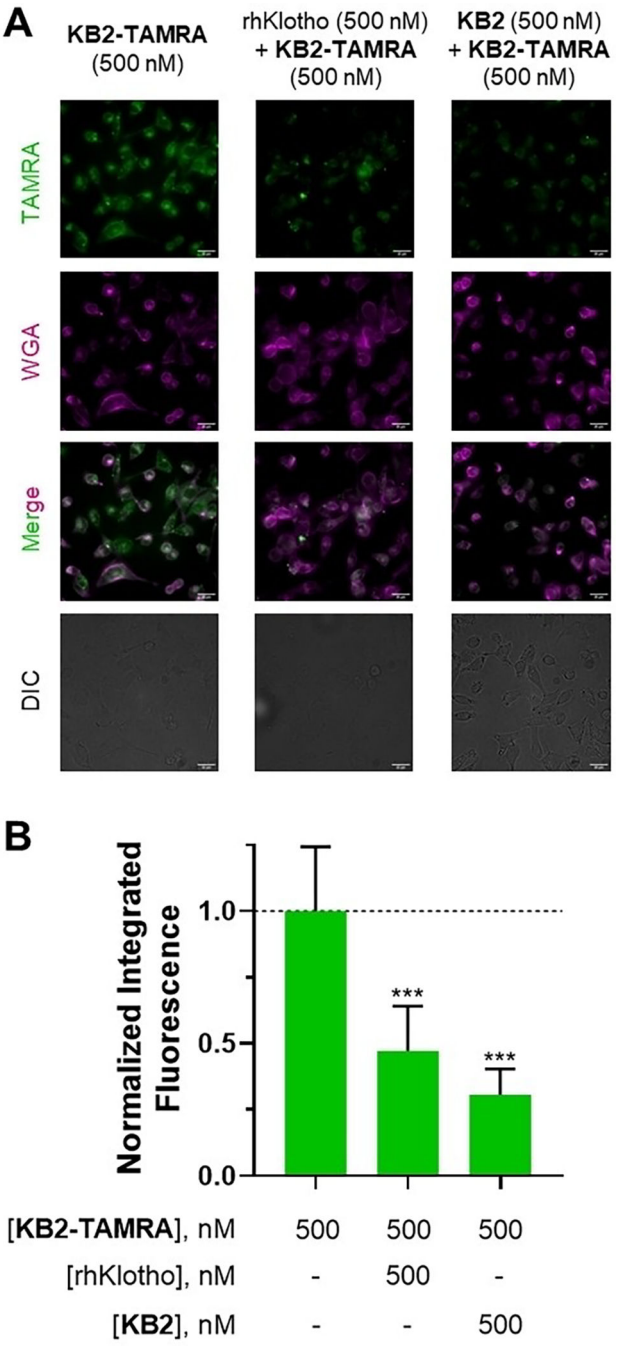

Figure 4.

Fluorescence microscopy imaging revealed target engagement of **KB2-TAMRA** labeling total Klotho in fixed HK-2 cells. (A) Left: detection of intracellular fluorescence and potential labeling of endogenous total hKlotho following 5 min of co-treatment with **KB2-TAMRA** at 500 nM and Wheat Germ Agglutinin (WGA) Alexa Fluor™ 350 Conjugate at 25 ng μL^{-1}. Fixation of cells was performed after the treatment. The fluorescence of **KB2-TAMRA** was acquired in the orange channel ($\lambda_{ex/em}$=542/597 nm). The fluorescence of WGA Alexa Fluor™ 350 was acquired in the blue channel ($\lambda_{ex/em}$=390/435 nm). Middle:

HK-2 cells treated for 5 min with a mixture of pre-incubated **KB2-TAMRA** (500 nM) and recombinant hKlotho (500 nM) displayed significantly decreased intracellular fluorescence. Right: HK-2 cells were pre-treated with **KB2** (500 nM) for 1 h, followed by co-treatment of **KB2-TAMRA** at 500 nM and WGA at 25 ng μL^{-1}. The pre-treatment of **KB2** also displayed significantly decreased intracellular fluorescence. Scale bar=25 μm. (B) The bar graph depicts the quantification of normalized integrated fluorescence in panel A (n=10). *** P<0.001, as determined by ANOVA. Error bars indicate SD.

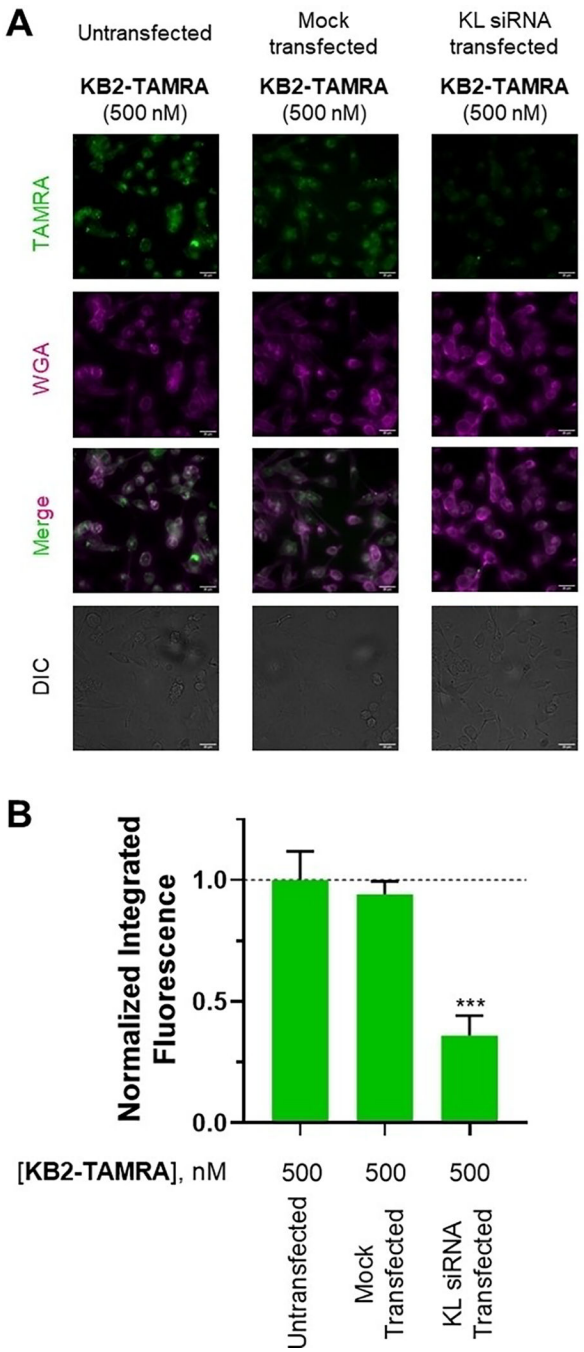

Figure 5.

Validation of the mode of action of Klotho labeling by **KB2-TAMRA** in fixed HK-2 cells. (A) In the first 2 columns, HK-2 cells were untransfected or mock-transfected by RNAiMAX reagents. In the last column, HK-2 cells were transfected with KL siRNA by RNAiMAX reagents. After transfection, **KB2-TAMRA** at 500 nM was co-treated with Wheat Germ Agglutinin (WGA) Alexa Fluor™ 350 Conjugate at 25 ng μL^{-1} in HK-2 cells. Fixation of cells was performed after the treatment. Fluorescence of **KB2-TAMRA** was acquired in the orange channel ($\lambda_{ex/em}$=542/597 nm). The Fluorescence of WGA Alexa

Fluor™ 350 was acquired in the blue channel ($\lambda_{ex/em}$=390/435 nm). Scale bar=25 μm. (B) The bar graph depicts the quantification of normalized integrated fluorescence (n=5). *** P<0.001, as determined by ANOVA. Error bars indicate SD.